JACS
JOURNAL OF THE AMERICAN CHEMICAL SOCIETY

A molecular replication process drives supramolecular polymerization

Yuanning Feng,[§] Douglas Philp*,[†]

[§] *Department of Chemistry, Northwestern University, 2145 Sheridan Road, Evanston, Illinois 60208, USA*
[†] *School of Chemistry, University of St Andrews, North Haugh, St Andrews, Fife KY16 9ST, UK*

*E-mail: d.philp@st-andrews.ac.uk

MAIN TEXT

***Correspondence Address**

Professor Douglas Philp
School of Chemistry
University of St Andrews
North Haugh
St Andrews, Fife KY16 9ST, UK
Tel: +44 (0)1334 467264
E-Mail: d.philp@st-andrews.ac.uk

ABSTRACT

Supramolecular polymers are materials in which the connections between monomers in the polymer main chain are non-covalent bonds. This area has seen rapid expansion in the last two decades and has been exploited in several applications. However, suitable contiguous hydrogen bond arrays can be difficult to synthesize, placing some limitations on the deployment of supramolecular polymers. We have designed a hydrogen bonded polymer assembled from a bifunctional monomer composed of two replicating templates separated by a rigid spacer. This design allows the autocatalytic formation of the polymer main chain through the self-templating properties of the replicators and drives the synthesis of the bifunctional monomer from its constituent components in solution. The template-directed 1,3-dipolar cycloaddition reaction between nitrone and maleimide proceeds with high diastereoselectivity affording the bifunctional monomer. The high binding affinity between the self-complementary replicating templates that allow the bifunctional monomer to polymerize in solution is derived from the positive cooperativity associated with this binding process. The assembly of the polymer in solution has been investigated by DOSY NMR spectroscopy. Both microcrystalline and thin films of the polymeric material can be prepared readily and have been characterized by powder X-ray diffraction and scanning electron microscopy. These results demonstrate that the approach described here is a valid one for the construction of supramolecular polymers and can be extended to systems where the rigid spacer between the replicating templates is replaced by one carrying additional function.

■ INTRODUCTION

Reports of supramolecular polymers[1-13] that exploit the action of carefully designed hydrogen bonding patterns to effect the controlled aggregation of monomer units first started to appear in the literature around 25 years ago. One of the most intensively studied monomer units that is capable of constructing a supramolecular polymer is based on the 2-ureido-4[1H]-pyrimidinone skeleton (**Figure 1a**, left). The critical recognition pattern is comprised of an array of two hydrogen bond donors (D) and two acceptors (A) in the order AADD. This hydrogen bonding pattern is self-complementary and allows the formation of homodimers in solution that are sufficiently stable ($K_a \sim 2 \times 10^7$ M^{-1}) to drive[14-17] supramolecular polymerization. Polymers that rely on the homodimerization of this recognition element have received significant attention[18-21]. However, this heterocyclic skeleton suffers[22-29] from a number of issues. Firstly, the synthesis[30-33] of heterocylic ring systems that contain large numbers of contiguous hydrogen bond donors or acceptors can be problematic. Therefore, one of the significant challenges in this field is the development of methodology that allows homodimeric systems with high association constants to be synthesized readily from simple building blocks. Secondly, tautomerization (**Figure 1a**, right) results in the formation of several alternate hydrogen bond arrays, only one of which is self-complementary—the structure that has a DADA hydrogen bonding pattern. This tautomerization process can affect[34-36] the material properties of any polymer based on this recognition system adversely. The tautomerization of the 2-ureido-4[1H]-pyrimidinone skeleton (**Figure 1b**, left, **UPy**) to form the corresponding pyrimidinol (**Figure 1b**, left, **UPyOH**). The pyrimidinol skeleton is self-complementary but possesses a much lower association constant ($K_a \sim 10^5$ M^{-1}) that is not considered sufficient to drive polymerization. We envisaged that we could construct a system containing four hydrogen bond donors and acceptors by appealing to the concept[37-41] of chelate cooperativity. The pattern of hydrogen bonds (DADA) found in the **UPyOH** tautomer (**Figure 1b**) possesses a K_a that is too low to facilitate the assembly of a supramolecular polymer. The low K_a is, in part, a consequence of the destructive secondary interactions[42] between the hydrogen bond donors and acceptors in this array.

Unlike **UPy** itself, which has one constructive secondary interaction (**Figure 1b**, right, green arrow), the DADA array present in **UPy-OH** possesses only destructive secondary interactions (**Figure 1b**, right, orange arrows).

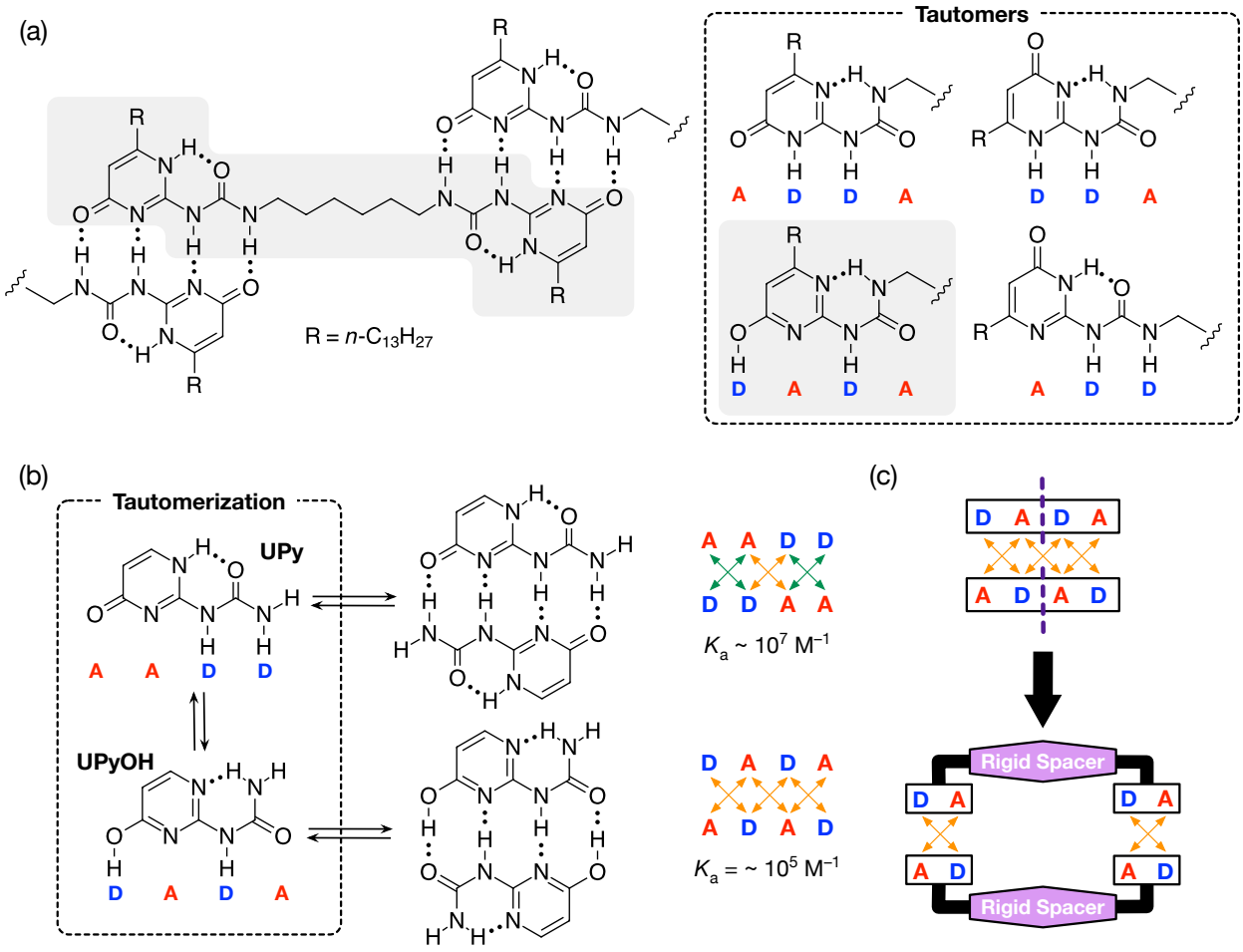

Figure 1. (a) A monomer (highlighted in gray) based on ureidopyrimidinone (UPy) assembling with other neighboring monomers through quadruple hydrogen bonds, in an AADD (A: Acceptor; D: Donor) array. (R^1 = *n*-$C_{13}H_{27}$) Other possible tautomers of UPy are shown in the box to the right. Only the DADA array (highlighted) is capable of forming self-complementary dimers. (b) The tautomerization equilibrium between UPy and the corresponding ureidopyrimidinol. The binding affinity of the quadruple [DADA•ADAD] hydrogen bond array present in the ureidopyrimidinol tautomer is significantly lower than that in the [AADD•DDAA] UPy tautomer. Unfavorable secondary hydrogen bond interactions (A ↔ A or D ↔ D), which lower the binding affinity of this complex, are indicated by orange arrows and the favorable secondary hydrogen bond interactions (D ↔ A or A ↔ D) are indicated by green arrows. (c) Schematic representation of the [DADA•ADAD] quadruple hydrogen bond array. This array can be separated into two isolated DA units that are then reconnected by a rigid spacer, removing the central unfavorable secondary interaction while retaining or enhancing its binding affinity.

Transforming this array by separating the DADA pattern into two isolated DA units that are connected by a rigid spacer (**Figure 1c**) removes the central destructive secondary interaction and, assuming the connection effective molarity[43] is > 1M, we can expect that this assembly will have a higher dimerization constant than the original contiguous DADA array. This strategy has the attraction of the far simpler synthesis of a self-complementary DA hydrogen bond diad and opens the prospect that the rigid spacer between these two diads might be synthesized using an auxiliary covalent bond forming step.

Our laboratory has described[Error! Reference source not found.–49] the use of small molecule templates to investigate the fundamentals of replication processes. We therefore proposed that it should be possible to combine the replication processes[Error! Reference source not found.–50] mediated by our synthetic templates with the assembly of supramolecular polymers. These processes are shown schematically in **Figure 2**. In order to exploit the high binding affinity of the template design shown schematically in **Figure 1c**, it is necessary to design (**Figure 2a**, top left) a system that connects two of these self-complementary units together. Initially, bistemplate **T** (**Figure 2a**) contains two self-complementary templates that are formed through the bimolecular reaction of bifunctional reagent **A** and monofunctional reagent **B**. Once **T** has been formed, it can use its recognition sites to create further copies of itself through a number of pathways. Bistemplate **T** can assemble reagents **A** and **B** into a ternary complex within Autocatalytic cycle 1 shown in **Figure 2a** (left). Pseudointramolecular reaction between **A** and **B** on **T** within the complex [**A•B•T**] creates a monofunctional template **T*** that can then be processed by the bifunctional template **T** in a second autocatalytic cycle (Autocatalytic cycle 2, **Figure 2a**, right). In this cycle, pseudointramolecular reaction between **T*** and **B** on **T** within the complex [**B•T*•T**] creates another copy of the bifunctional template **T**. Dissociation of the [**T•T**] complex allows the recycling of **T** into either of the two autocatalytic cycles shown in **Figure 2a** or assembly into a linear supramolecular **Polymer**. This polymer is catalytically active at its two termini (marked with ***** in **Figure 2a**) and can mediate the template directed reaction of **A** and **B** or **T*** and **B** at these termini (Catalytic cycle 3, **Figure 2a**). In addition, **T*** is capable of engaging in template directed

reactions (not shown in **Figure 2a**) involving **A** and **B** (→ **T***) or with **T*** and **B** (→ **T**). In summary, a rich network of template directed catalytic and autocatalytic processes can be created from the reaction of **A** and **B** that, ultimately, will result in the assembly of a supramolecular polymer by controlled aggregation of **T**.

The building blocks necessary to implement this reaction network are shown in **Figure 2b** and are designed readily by drawing on a replicator design[45] that has been exploited in several contexts by our laboratory. Bis-nitrone **A**, bearing amidopyridine recognition sites, can undergo sequential 1,3-dipolar cycloaddition reactions with two moles of maleimide **B**, bearing complementary carboxylic acid recognition sites, to afford, first, **T*** and, subsequently, template **T** (**Figure 2b**). The processes (**Figure 2a**), by which template **T** directs the formation of itself, is a formal replication cycle and template **T** is, in fact, an example of a self-replicator. A further feature of these template directed replication processes is the ability to use template **T** as an initiator for the polymerization process itself. The use of self-complementary templates as instructions in replication networks has been well-documented[51–55] previously by our laboratory.

An important design element in this system is the terphenyl spacer (**Figure 2b**) that connects the two cycloadducts in **T**. This spacer was chosen for two reasons. Firstly, two *n*-octyloxy substituents present in the center ring of the terphenyl unit afford the biscycloadduct excellent solubility in nonpolar organic solvents, such as chloroform, where hydrogen bonding between the recognition sites will be strongest. Secondly, the rigidity of the terphenyl unit prevents the self-complementary cycloadducts from complexing each other in an intramolecular sense. In this way, we ensure that the recognition sites that are ultimately required to mediate the formation of the cycloadduct, through the pathways shown in **Figure 2a**, are not already occupied by intramolecular complexation and, ultimately, should facilitate the supramolecular polymerization process shown in **Figure 2a**.

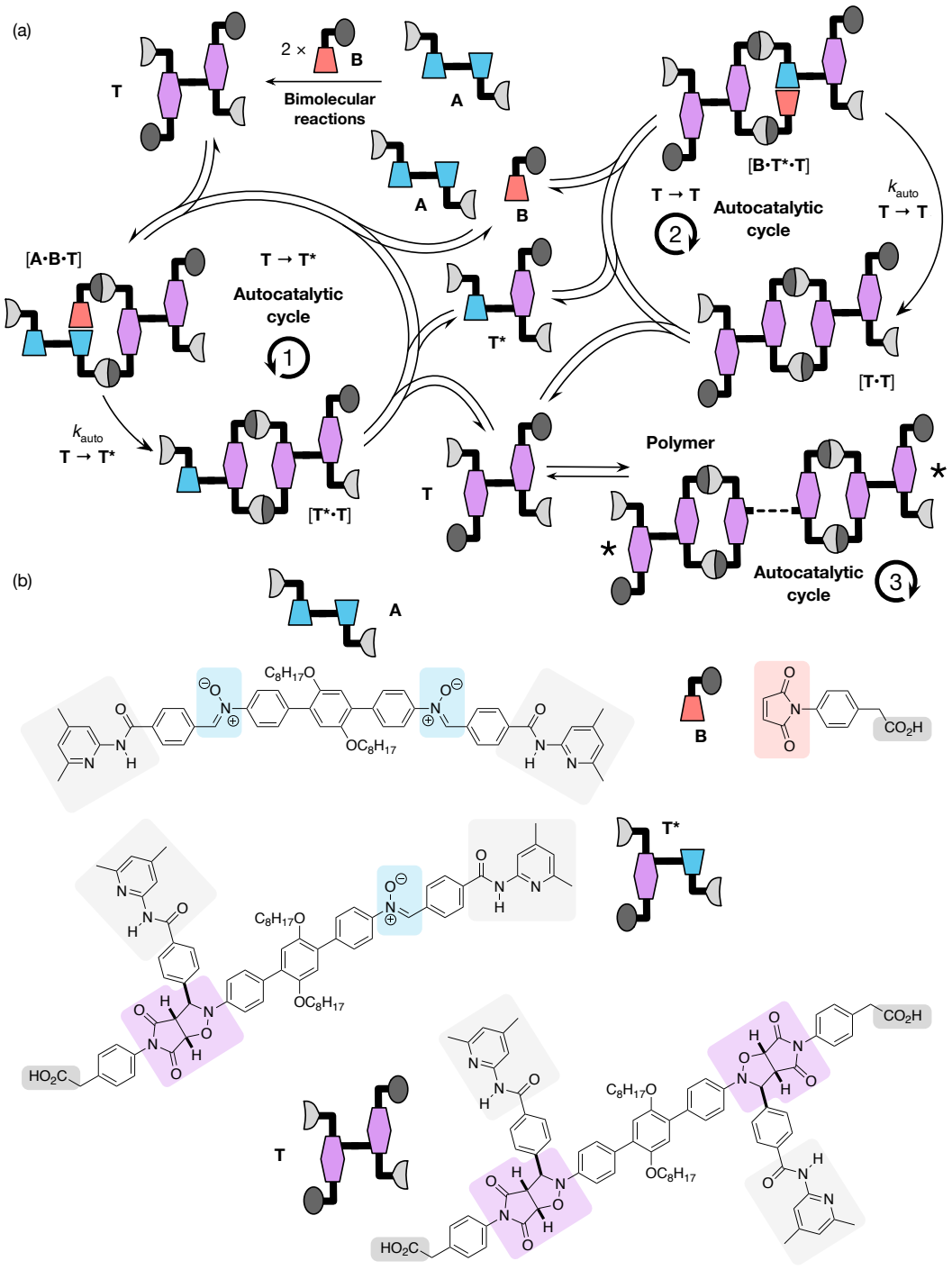

Figure 2. (a) Schematic representation of the reaction network created by reaction of the bifunctional reagent **A** and the monofunctional reagent **B** to create bistemplate T, which bears two self-complementary templates connected by a rigid spacer. This template can participate in a number of autocatalytic cycles in which **T** replicates itself. **T** can exploit the self-complementary nature of the two templates present in its structure to aggregate into a supramolecular **Polymer**. The ends of this polymer chain, marked *, are still active in a catalytic sense. For clarity, autocatalytic cycles that allow **T*** to replicate itself are not shown. (b) The chemical structures of building blocks **A** and **B** and templates **T*** and **T** required to implement the reaction network shown in (a).

The expectation that **T** will form a homodimer that is sufficiently stable to permit self-assembly into a polymer chain is derived from the concept[43,56] of chelate cooperativity. A monotopic binding event is characterized by a Gibbs energy of binding. In a system such as **T** that contains two such interaction sites that are connected covalently, the homodimer [**T**•**T**] will have a Gibbs energy of binding that is not necessarily equal to the simple sum of the Gibbs energy for the individual binding events. In a positively cooperative system, after the association of the first recognition site, the second site is in a favorable arrangement for binding to occur. In this case, the Gibbs energy of binding for the fully assembled system (ΔG^{12}) is more negative than the sum of the two individual binding events ($\Delta G^{1} + \Delta G^{2}$). The difference between these values is known as the connection free energy, ΔG^{S}, where $\Delta G^{S} = \Delta G^{1} + \Delta G^{2} - \Delta G^{12}$. A value of ΔG^{S} that is significantly greater than zero allows very stable complexes to be constructed from two relatively weakly bound recognition sites by exploiting positive cooperativity. Based on previous work[45,52,55,] in our laboratory, we anticipated that the *para*- disubstituted aromatic spacer units that separate the two recognition sites in each of the two templates present in **T** are sufficiently rigid and correctly oriented in order to ensure positively cooperative binding between **T** monomers in the growing polymer chain.

Here, we report a linear supramolecular polymer, based on these design principles, that can drive its own formation through catalytic and autocatalytic cycles involving a 1,3-dipolar cycloaddition reaction. We demonstrate that the monomer **T** can be used as an instruction for the formation of template through these catalytic processes. Kinetic analyses of the control and recognition-mediated pathways reveals that the template directed reaction within the hydrogen bonded complexes shown in **Figure 2** accelerates both the 1,3-dipolar cycloaddition as well as dramatically improving the diastereoselectivity of reaction affording the product, **T**, almost exclusively. DOSY NMR spectroscopic analysis demonstrates that the diffusion coefficient of the material present in solution decreases significantly as concentration is increased and temperature is decreased indicating that **T** assembles to form larger aggregates in solution under these conditions. In this polymer solution, the dynamic formation and cleavage of intermolecular hydrogen bonds allows the system to retain its ability to template its own formation. A film

can be grown from concentrated solutions of the polymer over extended periods and can be characterized by powder X-ray diffraction (PXRD) suggesting that the system develops a layered structure over extended periods of time. Scanning electron microscopy (SEM) images of samples cast from concentrated and dilute solutions of the polymer reveal that the film-like material is assembled from the concentrated solution, but not from the dilute solution.

■ RESULTS AND DISCUSSION

Kinetic Experiments

In order for our target system to be successful, we need to establish that the replicator at the core of our design retains the ability to template its own formation through an autocatalytic cycle (**Figure 3a**) using a model system that incapable of polymerization. To this end, we designed mono-nitrone **A′** (**Figure 3b**) by cutting the original bis-nitrone **A** in the middle of its rigid linker, whilst retaining two *n*-octyloxy chains in order to ensure solubility. The cycloadduct formed by the reaction of **A′** and **B**, namely **T′** (**Figure 3b**), will be structurally identical to one half of **T** and should have the ability to template its own formation through the intermediacy of the ternary complex [**A′•B•T′**] (**Figure 3a**).

Initially, in order to establish the background rate of the cycloaddition reaction in the absence of any recognition effects, maleimide **B′** (**Figure 3b**), in which the methylene carboxylic acid ($–CH_2COOH$) group has been replaced by a methyl ($–CH_3$) group that is incapable of recognition, was studied. Hence, maleimide **B′** was reacted with mono-nitrone **A′** in $CDCl_3$ ([**A′**] = 9.08 mM ; [**B′**] = 8.35 mM) at 10 °C and the reaction monitored by 400 MHz ^1H NMR spectroscopy for 16 h. Spectra were acquired at regular intervals during this period and then used to construct the concentration *vs.* time profile for the reaction shown in **Figure 3c** (filled red circles) by integration of the characteristic resonances arising from the cycloadduct in the region δ_H 4.0 to δ_H 6.0. The overall conversion to the major *trans*–**T″** cycloadduct was low, reaching 10 % after 16 h and the diastereoselectivity[FN] was poor — *trans* : *cis* ratio = 3.2 : 1.

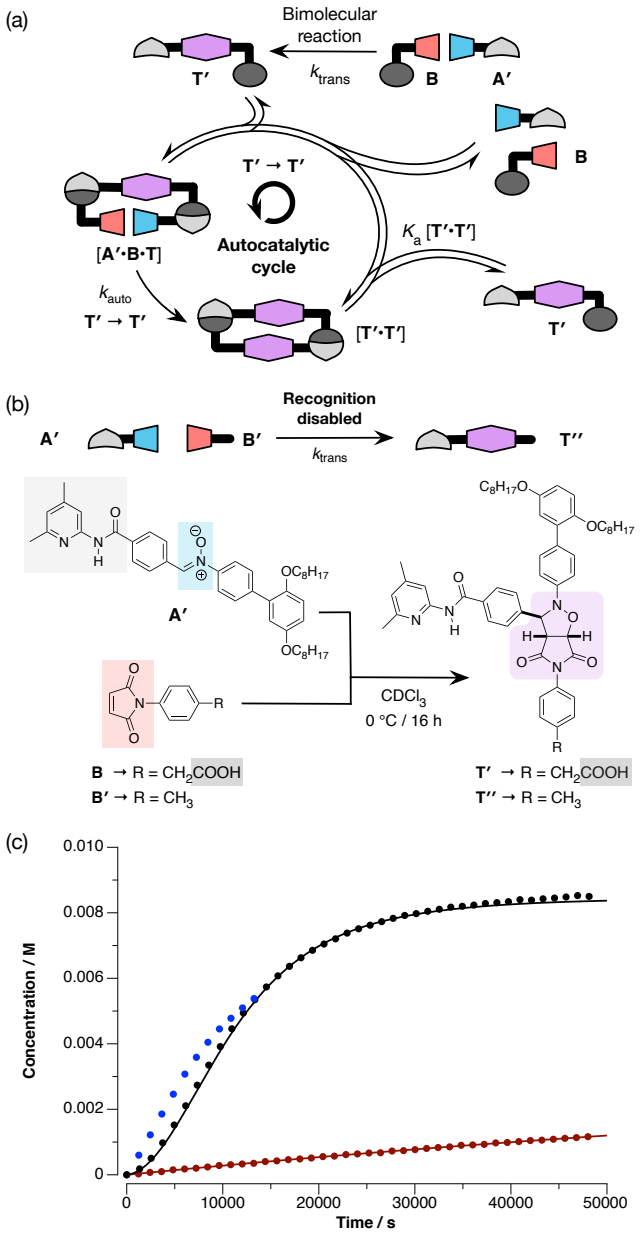

Figure 3. (a) Schematic representation of the self-replicating processes modelled by the monotopic template **T′**. Template **T′**, containing complementary recognition sites (light and dark gray) is formed initially through bimolecular reaction of **A′** with **B**. Once formed, **T′** can participate in a recognition-mediated autocatalytic cycle, where **T′** catalyzes the formation of a dimer [**T′•T′**] through the assembly of **A′** and **B** in the catalytically active ternary complex [**A′•B•T′**]. (b) Chemical structures of the compounds used in these kinetic studies, including the model of the bimolecular reaction **A′** + **B′** → **T″**. (c) Concentration-time plots for the reactions between **A′** + **B** → **T′** (black circles), the recognition disabled control reaction between **A′** + **B′** → **T″** (red circles) and **A′** + **B** → **T′** in the presence of 10 mol% added **T′** (blue circles). All reactions were performed in $CDCl_3$ at 283 K and 400 MHz ^{1}H NMR spectroscopy was used as the continuous assay. In the case of the reactions between **A′** + **B** → **T′** (black circles), **A′** + **B′** → **T″** (red circles) the solid lines represent the best fit of the kinetic data to the appropriate kinetic model (see Supporting Information for details). Data for the minor *cis* diastereoisomer is not shown for clarity.

Next, we assessed the reaction between mono-nitrone **A′** and maleimide **B**. These compounds were allowed to react in $CDCl_3$ at 10 °C ([**A′**] = 8.93 mM ; [**B**] = 8.45 mM) and, once again, the reaction monitored by 400 MHz ^{1}H NMR spectroscopy for 16 h. In this case, the reaction to form the isoxazolidine was significantly faster and the diastereoselectivity observed was enhanced dramatically — *trans* : *cis* ratio = 91 : 1. Additionally, the concentration *vs*. time profile for this reaction (**Figure 3c**, filled black circles) has a significantly sigmoidal shape that is characteristic of an autocatalytic process (template-directed replication). In order to confirm that **T′** is capable of templating its own formation, we performed an additional kinetic experiment in which mono-nitrone **A′** and maleimide **B** were allowed to react at in $CDCl_3$ at 10 °C ([**A′**] = 8.90 mM ; [**B**] = 8.15 mM) in the presence of 12 mol % (1.2 mM) of **T′**. Once again, this reaction monitored by 400 MHz ^{1}H NMR spectroscopy for 16 h and spectra were acquired at regular intervals during this period and then used to construct the concentration *vs.* time profile for the reaction shown in **Figure 3c** (blue circles). These data reveal that the lag period apparent in the time course for the reaction between mono-nitrone **A′** and maleimide **B** is now absent, providing conclusive evidence that **T′** can function as a template for its own formation.

In order to gain a deeper understanding for the efficiency of the replicator that is at the core of our polymer design, we subjected the kinetic data presented in **Figure 3** to simulation and fitting. In order to begin this process, we needed to derive the bimolecular rate constants for the reaction of mono-nitrone **A′** and a maleimide to afford either the *trans* or the *cis* cycloadduct. These rate constants can be estimated using the data (**Figure 3c**, red circles) obtained for the reaction of mono-nitrone **A′** and the control maleimide **B′**, which lacks a carboxylic acid recognition site. Kinetic data for this reaction can be fitted to a simple bimolecular model (see **Supporting Information**, **Section E**) and affords a rate constant (k_{trans}, **Figure 3a**) of 3.88×10^{-4} M^{-1} s^{-1} for the bimolecular formation of the *trans* cycloadduct — a value similar to those we have reported previously[45,52,55] for similar systems, indicating that the *N*-aryl substituent present in mono-nitrone **A′** has no significant effect on the electronics of the 1,3-dipole. In order to proceed with the fitting of the data from the recognition-enabled experiment, it was

necessary to determine the single point association constant for the binding of the amidopyridine recognition site on the nitrone to the carboxylic acid recognition site on the maleimide. Monitoring of a titration of maleimide **B** with a suitable model amidopyridine (compound **S6)** using isothermal titration calorimetry (see **Supporting Information**, **Section F**) afforded a value of 1500 M^{-1}. This value, along with the rate constant for the bimolecular cycoaddition were then used to fit the recognition-enabled data for the reaction **A′** + **B** → **T′** to the appropriate kinetic model in order to obtain values of the autocatalytic rate constant (k_{auto}, **Figure 3a**) and the association constant (K_a[**T′• T′**], **Figure 3a**) for the template duplex. The rate constant k_{auto} is associated with the reaction to form the cycloadduct that takes place within the catalytically active ternary complex [**A′•B•T′**] and is a measure of the efficiency of the replicator **T′**. The equilibrium constant K_a[**T′• T′**] measures the stability of the product duplex [**T′•T′**] that is formed by reaction within [**A′•B•T′**] and will, ultimately, influence the stability of the polymer than is constructed from such duplexes. The equilibrium between the product duplex [**T′•T′**] and monomeric **T′** determines the amount of free autocatalyst present in the system at any given time point and will therefore affect the efficiency of the replication process directly. Additionally, it is this equilibrium that drives the formation of the supramolecular polymer that assembles from monomer **T**. Fitting the data from the reaction between mono-nitrone **A′** and maleimide **B** (black filled circles, **Figure 3c**) afforded a good fit of the experimental data (**Figure 3c**) to the appropriate kinetic model (see **Supporting Information**, **Section G** for details of the fitting process). The best fit value of k_{auto} (6.23×10^{-3} s^{-1}), together with that for bimolecular rate constant for this cycloaddition obtained previously, allows us to estimate the kinetic effective molarity (kEM) achieved by the catalytic ternary complex [**A′•B•T′**]. The value of kEM obtained (16.1 M) is in the range expected for replicating templates in this class and indicates that the addition of large solubilizing groups to the nitrone *N*-aryl substituent do not have any significant effect on the efficiency of replication. The value of K_a[**T′• T′**] obtained from this fitting process (5.92×10^6 M^{-1}) indicates that the [**T′•T′**] duplex benefits from significant positive cooperativity (connection effective molarity = 2.63 M, connection free energy = 2.3 kJ mol^{-1}) and its stability is in the range required for the successful assembly of the supramolecular polymer.

Having established that the replicator design at the core of our system was viable, we next turned to assessing the performance of bistemplate **T** in templating its own formation. Accordingly, we prepared mixtures of **A** and **B** in $CDCl_3$ ([**A**] = 10 mM; [**B**] = 20 mM) and allowed these mixtures to react at 10 °C for different time periods ranging from 1 hour up to 21 hours. After the appropriate time, CD_3SOCD_3 was added to one of these samples in order to quench recognition-mediated reaction by disrupting any hydrogen bond mediated reactions in the system and the conversion of **A** and **B** to **T** in this sample was then assayed using 500 MHz ^{1}H NMR spectroscopy (see **Supporting Information, Figure S17**). After 21 hours, the conversion of **A** and **B** to **T** is significantly lower than the reaction between **A′** and **B** to form **T′** (54 % vs. 72 %). In addition, the diastereoselectivity observed in the formation of **T** (*trans* : *cis* = 37:1) is lower than in the case of the model system **T'** (*trans* : *cis* = 91:1).

At this stage, it was important to demonstrate that, in common with the model replicating template **T′**, **T** itself could instruct its own formation. To this end, we performed an experiment in which a $CDCl_3$ solution was prepared containing **A** (10 mM), **B** (10 mM) and **T** (10 mol%, 1 mM). This solution was allowed to react at 10 °C sampled at various time points over the course of 21 hours. Once again, each sample was diluted with CD_3SOCD_3 in order to quench recognition mediated reaction by disrupting any hydrogen bonding present in the system and assayed by 500 MHz ^{1}H NMR spectroscopy (**Figure 4**). After 1 hour, the conversion of **A** and **B** to **T** in the presence of 10 mol% added **T** experiment is 3.1 % compared to 1.9 % in the original experiment where no **T** was added initially. The overall conversion to **T** after 21 hours in the presence of 10 mol% added **T** is 67% (*cf.* 54% in the absence of added **T**). In addition, the diastereoselectivity improved in the presence of 10 mol% added **T** to 45:1 in favor of *trans* (*cf.* 37:1 in the absence of added **T**). These results clearly establish that, despite the greater number of pathways in the reaction network associated with the formation of **T**, bistemplate **T** is indeed capable of acting as a catalyst for its own formation as set out in our original design shown in **Figure 2**.

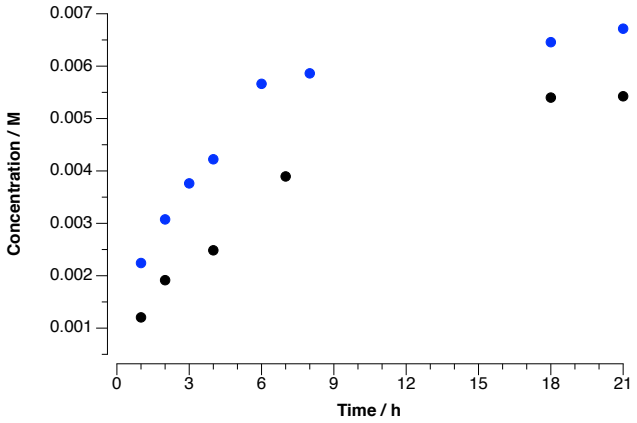

Figure 4. Concentration-time plots for the reactions between **A** and **B** → **T** ([**A**] = 10 mM; [**B**] = 20 mM) performed in $CDCl_3$ at 283 K either in the absence of added **T** at the start of the reaction (black circles) or in the presence of 10 mol% added **T** at the start of the reaction (blue circles). In both cases, a discontinuous assay was used. Each sample was diluted with CD_3SOCD_3 (100 μL) to quench recognition mediated reaction through disrupting hydrogen bonding in the system and then analyzed by 500 MHz ^{1}H NMR spectroscopy to determine composition of the mixture.

It is instructive at this point to consider the bimolecular reaction pathways leading from **A** and **B** to **T** with those connecting **A′** and **B** to **T′**. When **A** and **B** are mixed at the start of the experiment, the 1,3-dipolar cycloaddition must proceed through a bimolecular template-independent pathway as there is no template **T** present in solution at this time to catalyze its own formation. This bimolecular reaction exhibits relatively poor diastereoselectivity (*trans* : *cis* ~ 3:1) when compared with the template directed process (*trans* : *cis* ≥ 30:1). For the cycloaddition between mono-nitrone **A′** and **B**, 75 % (3 out of 4) of the cycloadducts formed by the bimolecular process are **T′**, which is capable of acting as a template for its own formation. By contrast, the reaction between **A** and **B** has significantly more stereochemical outcomes. Since **A** is a bis-nitrone, it can undergo two independent cycloaddition reactions. We must consider the outcome of both of these cycloadditions to determine how quickly **T** (containing two *trans* cycloadducts) becomes available to drive the template directed process. In fact, statistically, the bimolecular pathways available to the reaction between bis-nitrone **A** and **B** result in a ratio of the product cycloadducts—*trans*-*trans* (**T**), *trans*-*cis* and *cis*-*cis*—of 9:6:1. Whilst the *cis*-*cis* product cannot act as a template in any sense, the *trans*-*cis* isomer has one cycloadduct

with the correct stereochemistry (*trans*) to act as a template for the production of further *trans* cycloadducts. Therefore, the bimolecular, template independent processes available to the reaction between bis-nitrone **A** and **B** affords more viable template per unit time (94% — 15 out of 16 possibilities) than that for the cycloaddition between mono-nitrone **A′** and **B** (75% — 3 out of 4 possibilities). This consequence of this effect should manifest itself as a shortening or disappearance of the lag period normally observed for an autocatalytic reaction. This hypothesis can be supported tentatively by the pseudokinetic data recorded (**Figure 4**) for the reaction between **A** and **B** described above, which, unlike the formation of **T′** from **A′** and **B** (**Figure 3c**, black circles), does not display an obvious lag period. It is possible that, at later time points, the template effect may be attenuated in the case of the polymer system as a consequence of the assembly of the template **T** into hydrogen-bonded polymer chains (**Polymer**, **Figure 2a**). The polymerization process will reduce the amount of free **T** available to the system as, effectively, the template effect is only operational at the ends of the polymer chains. This attenuation of the template effect is expected to increase with increasing conversion of the nitrone and maleimide to cycloadduct as the degree of polymerization (DP) increases and the number of chain ends diminishes.

DOSY NMR Spectroscopy

In order to gain some insight into the self-assembly processes accessible to ditopic template **T** we turned to diffusion-ordered spectroscopy (DOSY). In order to establish the formation of the supramolecular polymer derived from **T**, it was also necessary to study the behavior of monotopic template **T′** under identical conditions. Accordingly, we performed DOSY experiments (**Figure 5**) on samples of monotopic **T′** and ditopic **T** across the concentration range 5 to 80 mM in $CDCl_3$ at temperatures from +20 °C down to –20 °C. We expected that in the case of monotopic **T′**, there would be a limited difference in the observed diffusion coefficient across the concentration range as there was no possibility for this monomer to self-assemble into supramolecular aggregates that are larger than the homodimer [**T′•T′**]. By contrast, ditopic **T** was expected to exhibit a

marked decrease in its observed diffusion coefficient as concentration was increased as a consequence of the self-assembly process. Additionally, we expected that lowering the temperature would have a more marked effect on the observed diffusion coefficient for monomer **T** since these conditions favor supramolecular aggregation. The results obtained in these experiments are summarized in **Figure 5**.

It is clear from these data that the diffusion coefficients observed for ditopic template **T** (pale red → dark red circles (+20 °C → –20 °C)) are strongly dependent on both the concentration of the $CDCl_3$ solution and temperature at which the DOSY experiment was performed. At 20 °C (pale red circles), the most dilute solution of **T** (5 mM in $CDCl_3$) affords a diffusion coefficient of 2.69×10^{-10} m^2 s^{-1}. Increasing the concentration to 80 mM results in the observed diffusion coefficient for **T** decreasing by an order of magnitude to 2.46×10^{-11} m^2 s^{-1}. When the temperature was decreased to –20 °C (dark red circles), the diffusion coefficients at 5 mM and 80 mM were again different by an order of magnitude (1.28×10^{-10} m^2 s^{-1} at 5 mM and 1.16×10^{-11} m^2 s^{-1} at 80 mM). In addition, the diffusion coefficients measured at –20 °C are uniformly lower compared to those measured at +20 °C. By contrast, the observed diffusion coefficients determined, under the same conditions, for the monotopic template **T′** (black squares, +20 °C) did not show a strong dependence on the concentration of the solution. For example, at +20 °C (black squares), our DOSY analysis of a solution of **T′** in $CDCl_3$ afforded a diffusion coefficient of 4.90×10^{-10} m^2 s^{-1} at 5 mM and 3.46×10^{-10} m^2 s^{-1} at 80 mM. When the temperature was decreased to –20 °C, a similar limited dependence on concentration was observed—at 5 mM, the observed diffusion coefficient for **T′** was 2.78×10^{-10} m^2 s^{-1} compared with 1.71×10^{-10} m^2 s^{-1} at 80 mM.

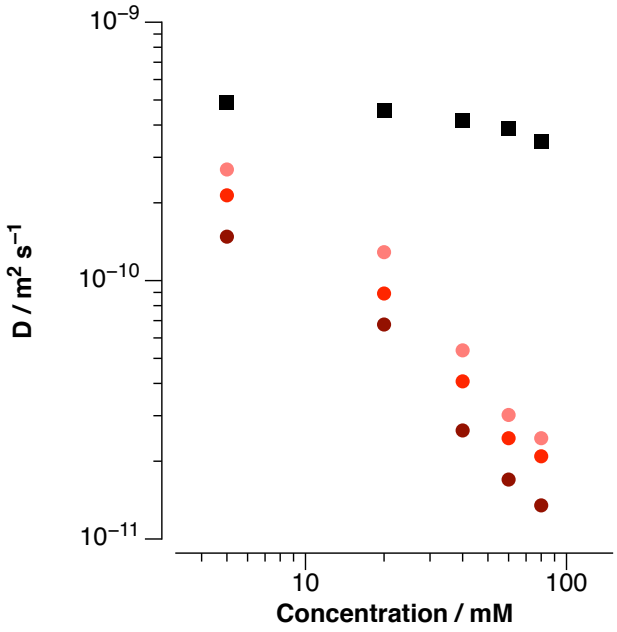

Figure 5. Plot of the diffusion coefficients, determined by DOSY NMR spectroscopy, as a function of concentration for monotopic template **T′** (black squares) and ditopic template **T** (pale red circles) at +20 °C in $CDCl_3$ solution. The red and dark red circles represent the diffusion coefficients determined for **T** at +10 °C and –10 °C, respectively.

Taken together, these results suggest strongly that our hypothesis is correct and that ditopic template **T** is capable of forming extended structures in solution. DOSY NMR spectroscopy is, however, unable to afford any detailed structural information on these assemblies, hence, in order to gain some insight into these structures, we turned techniques that could probe these assemblies in the solid state.

Powder X-Ray Diffraction (PXRD)

A series of polymer **T** solutions at various concentrations from 5 mM to 80 mM in $CDCl_3$ were aged at 298 K for 100 days. After this time, some dark colored material (**Figure S32**) had appeared in the more concentrated solutions ($c \geq 40$ mM). A yellow-orange **Film** could be recovered from the 40 mM solution and this material was compared with a sample (**Powder**) of polymer **T** that had been prepared by simply drying completely the material obtained after reaction of **A** and **B** in $CDCl_3$ for 7 days, affording a powder (**Figure S32**). This comparison was carried out by removing the **Film** from the solution with a needle and placing this material on top of a Kapton (polyimide) tape (**Figure S33**). For comparison purposes, a sample of the **Powder** was mounted on Kapton tape

separately. These samples and an additional **Background** sample, which only had the Kapton tape, were analyzed using PXRD (See **Section I** in **Supporting Information** for further details).

The microdiffraction patterns recorded on these samples indicate that the properties of the **Film** sample are markedly different from those of the **Powder** sample. Whilst the **Powder** sample affords a largely featureless diffraction pattern (**Figure 6a**) that is similar to that of the **Background** sample, the **Film** affords a diffraction pattern that exhibits a series of relatively well-resolved reflections (**Figure 6b**). Interestingly, a number of these reflections (labelled **1** → **3** in **Figure 6b**) occur at *d* spacings that are exact multiples of each other. This observation is suggestive of the development of a layered structure within the film. We attribute the dramatic difference between the **Film** sample and the **Powder** sample to a slow aging process that allows the polymer chains to become oriented in solution. Rapid removal of the solvent from the sample when preparing the **Powder** does not give the polymer chains an adequate opportunity to become aligned and, thus, no order can develop within the material. By contrast, the extremely slow aging of the sample from which the **Film** was removed, afforded the opportunity for the development of long-range order within the material as evidenced by the relatively well resolved diffraction pattern. This behavior is also evident in other respects. Solutions of **T** in $CDCl_3$ at 80 mM, either in NMR tubes or in vials, become extremely viscous (**Figure S35**) after standing for at least 7 days. These samples do not develop these gel-like properties in less than this time. This observation suggests that the order in the sample detected by PXRD develops very slowly.

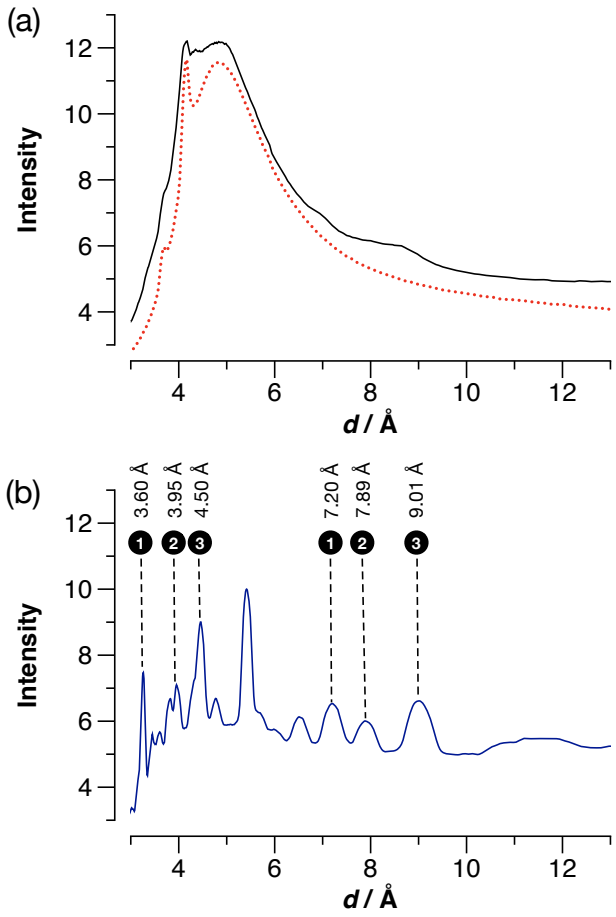

Figure 6. PXRD patterns, plotted as distance *vs.* intensity, obtained from (a) the **Powder** sample of **T** (black). (b) the **Film** sample of **T** (blue). The background associated with the polyimide tape used to mount each sample is the dashed red line in (a). Some reflections are marked for comparison purposes.

Scanning Electron Microscopy (SEM)

The assembly of supramolecular polymers are associated with a key concentration known as the critical polymerization concentration[57–62] or CPC. At concentrations below the CPC, the system will exist primarily as rings containing two or more monomers. As the concentration increases these rings will tend to diminish in concentration and linear polymer chains will begin to dominate. At concentrations well above the CPC, it is the linear polymer that is dominant in solution. We would therefore expect that the properties of the solvent, such as viscosity, will be affected significantly as the concentration of **T** increases in $CDCl_3$ solution. Curiously, significant effects on the properties of solutions of **T** were only observed when samples were allowed to stand for significant periods of time.

We have already noted the formation of film-like material in more concentrated solutions of **T** (≥ 40 mM). We prepared six samples of **T** dissolved in $CDCl_3$ at a range of concentrations from 5.0 mM to 80 mM (**Figure 7a**, left). When these solutions were prepared initially, there was no discernible difference in their viscosity visually or by analytically—measurement of the viscosity of freshly prepared solutions of **T** in $CDCl_3$ using an Anton Paar® MCR 302 rheometer revealed little difference in their viscosities across the concentration range 5 mM to 80 mM. However, on leaving the set of six vials to stand for 100 days, marked differences in the viscosity of the solutions developed. As we had expected initially, the more concentrated solutions had become significantly more viscous—indeed, the 80 mM solution was now so viscous that it could support its own weight both in an NMR tube (**Figure 7a**, right) and in a vial. Interestingly, although the samples in the vials had been aged for 100 days, the NMR tube had only stood for 7 days, suggesting that the timescale of the aging process may be on the order of days rather than weeks. We had determined from the powder X-ray diffraction experiments that after 100 days; the sample contained an organized network of self-assembled **T** monomers. The formation of this network is most likely responsible for the change in the properties of solutions that we had prepared. However, it was not clear if there was any assembly processes that were occurring in the freshly prepared solutions of **T**. In order to probe for the presence of self-assembly in the freshly prepared solution of **T**, we turned to scanning electron microscopy (SEM). We prepared three sets of samples on silicon substrates, spotting solutions containing different concentrations of **T**—1.0 mM, 10 mM and 80 mM—in $CDCl_3$ on to the silicon and allowing the spots to dry. We envisaged that at the lowest concentration, where, based on the behavior of the aged vial samples, the solution would contain little linear polymer, we would deposit material[63] that was essentially microcrystalline in nature. By contrast, based on the behavior of the aged vial samples, we anticipated that the highest concentration studied (80 mM) would contain most linear polymer. Therefore, the material deposited on the substrate would be expected to be film-like.

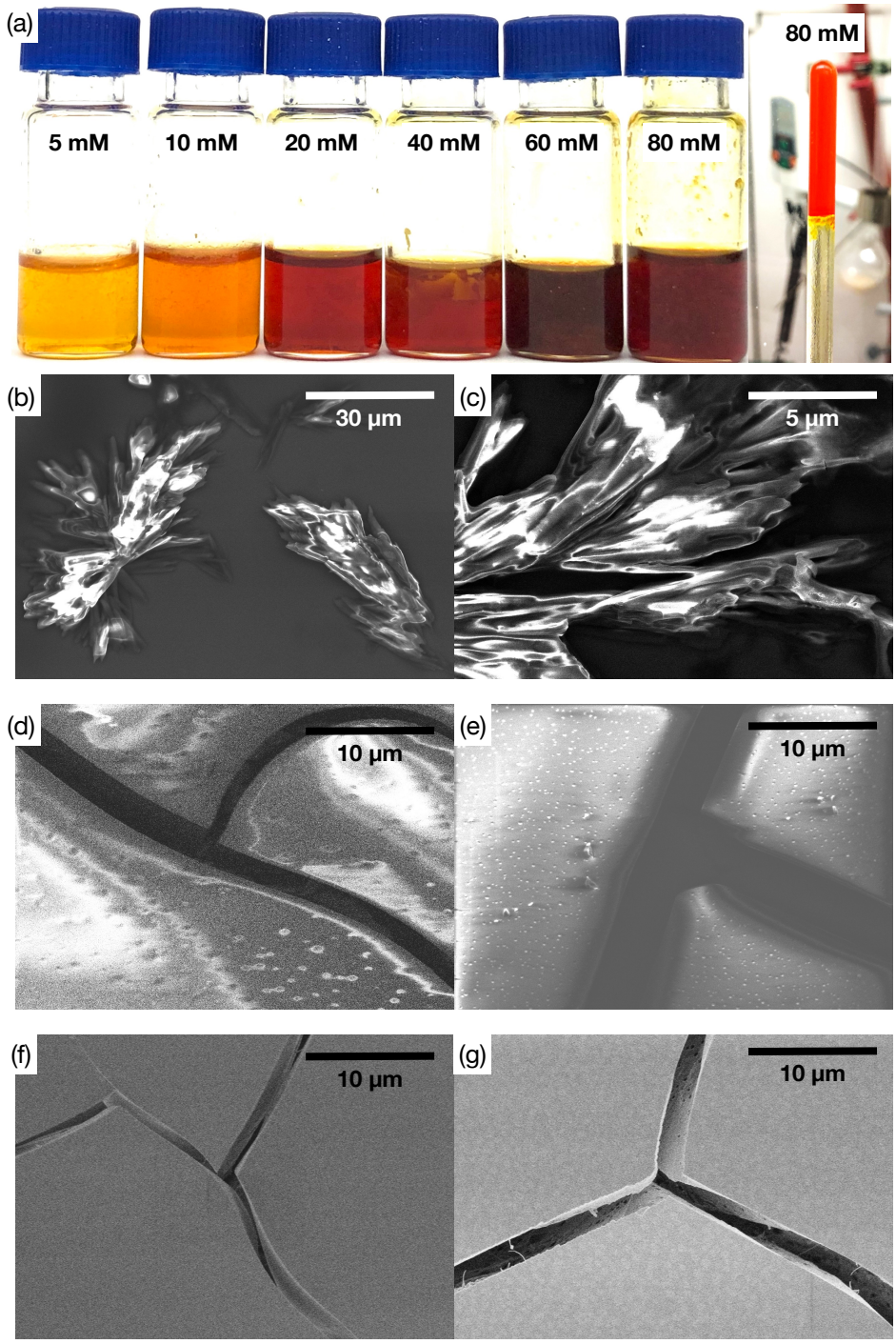

Figure 7. (a) Left: Vials containing samples of **T** dissolved in $CDCl_3$ at a range of concentrations at room temperature and aged for 100 days. The material used to record the PXRD data shown in Figure 6 was obtained from the 40 mM sample shown here. Right: Inverted NMR tube containing an 80 mM solution of **T** in $CDCl_3$ that had been aged for 7 days demonstrating the dramatic change in viscosity of this sample. (b → g) Scanning electron micrographs of samples deposited on a silicon substrate from solutions of **T** in $CDCl_3$ at 298 K at concentrations of (b,c) 1 mM, (d,e) 10 mM and (f,g) 80 mM.

We expected that the 10 mM sample might exhibit the same behavior as either sample depending on the exact degree of polymerization at this concentration. Imaging of the sample prepared from the 1.0 mM solution (**Figure 7b** and **c**) reveals μm-sized microcrystallites, suggesting that, at this concentration, the sample does not contain significant amounts of linear polymer. By contrast, imaging of both the sample prepared from the 10 mM solution and that prepared from the 80 mM solution revealed smooth films on the surface of the substrate (**Figure 7d** and **e**, 10 mM; **Figure 7f** and **g**, 80 mM). The films in these two samples had similar morphologies, however, that formed from the 80 mM solution was, not unexpectedly, thicker. These results suggest that even in freshly prepared solutions of **T**, there may be a significant amount of the linear supramolecular polymer present at concentrations of 10 mM or higher. However, the mechanism of the transition in the properties of these samples between 1 day and 100 days is not yet understood.

■ CONCLUSION

In this work, we have demonstrated a valid design strategy for the assembly of a supramolecular polymer based on a template-directed replication process. Reaction of a bis-nitrone containing two amidopyridine recognition sites and a rigid *p*-terphenylene spacer with a maleimide bearing a carboxylic acid recognition site affords a monomer **T** that contains two cycloadducts that are capable of self-association to form a stable dimer. Kinetic studies demonstrate that the recognition sites present in **T** and its constituent components, **A** and **B**, are capable of accelerating the cycloaddition reaction between **A** and **B** significantly (effective molarity > 10 M) and that the reactions to form the monomer **T** proceed with a high degree of diastereoselectivity (dr > 30 : 1). Despite the self-complementarity between in the two cycloadducts present in **T**, the presence of the rigid *p*-terphenylene spacer prevents self-association occurring in an intramolecular sense. Instead, the monomer **T** assembles in $CDCl_3$ at 10 °C to afford a linear, hydrogen bonded polymer chain. This assembly process has been characterized in solution using DOSY NMR spectroscopy, which demonstrates that the polymerization process is favored by high concentration and low temperature. On standing, solution of **T** above 40 mM form a film-like material which has been characterized by powder X-ray diffraction. This

technique reveals that the structure of this material matches well with a computational model of the polymer chain. The polymer also forms smooth films on evaporation of a dilution solution in $CDCl_3$ that can be imaged by scanning electron microscopy.

The work presented here represents a proof-of-concept—we have demonstrated that it is possible to couple[64–74] a molecular level processes, such as replication processes, with the formation of a supramolecular material. The spacer utilized in this system is essentially inert and is used simply for its rigid molecular framework. Replacement of this spacer with more complex functional structures opens the way to make designer materials whose formation can be instructed using the template-directed approach outlined here. Additionally, introduction of spacers that have higher connection numbers than two, *e.g.,* trifunctional or tetrafunctional, offers the opportunity to construct two-dimensional or three-dimensional structures rather than a one-dimensional, linear polymer chain. Finally, coupling of the replication process to a dynamic covalent library offers the prospect of creating a number of different polymers to order from the same equilibrating mixture of starting materials simply by instructing the library using an instructional template.

■ ASSOCIATED CONTENT

The Supporting Information is available free of charge at https://pubs.acs.org/doi/xxxx/jacsxxx.

Details of synthetic procedures, measurement of diffusion coefficients using DOSY NMR spectroscopy, mass spectrometry, kinetic experiments, simulation and fitting, isothermal titration calorimetry measurements and powder X-Ray diffraction experiments.

■ AUTHOR INFORMATION

Corresponding Author

Douglas Philp – School of Chemistry, University of St Andrews, North Haugh, St Andrews, Fife KY16 9ST, UK; orcid.org/ 0000-0002-9198-4302; Email: d.philp@st-andrews.ac.uk

Author

Yuanning Feng – Department of Chemistry, Northwestern University, Evanston, Illinois 60208, USA; orcid.org/0000-0002-8832-0767

Notes

The authors declare no competing financial interest.

■ ACKNOWLEDGMENTS

The authors thank Northwestern University (NU) for their support of this research. We would also like to thank Dr. Christos Malliakas and Dr. Elizabeth King for their assistance with the collection of PXRD and SEM data. This research made use of the IMSERC NMR, MS and PXRD facility at Northwestern University, which has received support from the Soft and Hybrid Nanotechnology Experimental (SHyNE) Resource (NSF ECCS-2025633) and Northwestern University. This research made use of the EPIC SEM facility of Northwestern University's NUANCE Center, which has received support from the SHyNE Resource (NSF ECCS-2025633), the IIN, and Northwestern's MRSEC program (NSF DMR-1720139).

■ EXPERIMENTAL SECTION

Synthesis

Compounds **A** and **A′** were synthesized using standard procedures from commercially available starting materials. The synthetic routes employed are shown in **Schemes S1** to **S3** in the **Supporting Information** along with detailed procedures describing these routes. Compounds **B** and **B′** were prepared using literature procedures.

The bis-isoxazolidine monomer **T** was synthesized from bis-nitrone **A** and maleimide acid **B** was prepared by a 1,3-dipolar cycloaddition performed in $CDCl_3$ at –24 °C (see **Scheme S4**). The mono-isoxazolidine template **T′** was synthesized from mono-nitrone **A′** and maleimide acid **B** was prepared by a 1,3-dipolar cycloaddition performed in $CDCl_3$ at –24 °C in an identical manner to that employed for bis-isoxazolidine monomer **T**. Further experimental details are provided in **Section B** of the **Supporting Information**.

Kinetic Experiments

A 10 mM stock solution 2,4-dinitrotoluene (the internal standard) in $CDCl_3$ was prepared at room temperature. This solution was then used to dissolve the appropriate amounts of nitrone **A′** and either **B** or **B′** depending on the data to be recorded. In one experiment, 10 mol% of **T′** was also dissolved in the solution. Once the solution containing all of the starting materials had been prepared, the solution was transferred to an NMR tube, fitted with a polyethylene cap to prevent solvent evaporation and then transferred to a 600 MHz ^{1}H NMR spectrometer which had been pre-equilibrated to 283 K. Spectra were then recorded at 20 minute intervals for 16 hours. Data for the reaction between nitrone **A′** and **B** (**Figure S12**), between nitrone **A′** and **B′** (**Figure S15**) and reaction between nitrone **A′** and **B** in the presence of 10 mol% **T′** (**Figure S14**) are provided, together with other experimental details, in **Section E** of the **Supporting Information**.

DOSY NMR Spectroscopy

A solution of compound **T** at 80 mM was prepared in a 20-mL scintillation vial using fresh $CDCl_3$ with sonication at room temperature. The solution was divided into five portions and four of these were diluted further using fresh $CDCl_3$ affording solutions with

concentrations of 60 mM, 40 mM, 20 mM and 5 mM concentrations, respectively. Each solution was transferred into a Wilmad™ thin-walled high-throughput NMR tube and sealed with a polyethylene pressure cap to avoid solvent evaporation. Each tube was transferred to an NMR spectrometer (Bruker Neo 600 MHz instrument with a temperature regulated CP QCI 600S3 H/F-C/N-D-05 Z cryoprobe). DOSY data was acquired at each concentration at the following temperatures 20 °C, 10 °C, 0 °C, –10 °C and –20 °C. The pulse program used was dstebpgp3s (swh = 9615.38 Hz (16.0309 ppm); ns = 16) and the parameters Δ (d20, diffusion delay) and δ (p30, diffusion gradient pulse) were optimized for each sample. Further experimental details are provided in **Section H** of the **Supporting Information**.

Powder X-Ray Diffraction (PXRD)

PXRD data were collected at room temperature on a STOE-STADI-P powder diffractometer equipped with an asymmetric curved Germanium monochromator (CuKα1 radiation, λ = 1.54056 Å) and one-dimensional silicon strip detector (MYTHEN2 1K from DECTRIS). The line focused Cu X-ray tube was operated at 40 kV and 40 mA. sample was packed in a 3 mm metallic mask and sandwiched between two layers of polyimide tape. Intensity data from 1.5 to 30° 2θ were collected over a period of 50 minutes. Instrument was calibrated against a NIST Silicon standard (640d) prior the measurement. Further experimental details are provided in **Section I** of the **Supporting Information**.

■ REFERENCES

1 Brunsveld, L.; Folmer, B. J. B.; Meijer, E. W.; Sijbesma, R. P. Supramolecular Polymers. *Chem. Rev.* **2001**, *101*, 4071–4098.

2 Lehn, J.-M. Supramolecular Polymer Chemistry—Scope and Perspectives. *Polym. Int.* **2002**, *51*, 825–839.

3 Lehn, J.-M. Dynamers: Dynamic Molecular and Supramolecular Polymers. *Prog. Polym. Sci.* **2005**, *30*, 814–831.

4 Binder, W. H.; Zirbs, R. Supramolecular Polymers and Networks with Hydrogen Bonds in the Main and Side-Chain. In: *Hydrogen Bonded Polymers*; Binder, W. H., Ed.; Springer-Verlag Berlin Heidelberg: Berlin and Heidelberg, Germany, **2007**; pp 1–78.

5 De Greef, T. F. A.; Meijer, E. W. Supramolecular Polymers. *Nature* **2008**, *453*, 171–173.

6 De Greef, T. F. A.; Smulders, M. M. J.; Wolffs, M.; Schenning, A. P. H. J.; Sijbesma, R. P.; Meijer, E. W. Supramolecular Polymerization. *Chem. Rev.* **2009**, *109*, 5687–5754.

7 Aida, T.; Meijer, E. W.; Stupp, S. I. Functional Supramolecular Polymers. *Science* **2012**, *335*, 813–817.

8 Liu, K.; Kang, Y.; Wang, Z.; Zhang, X. 25th Anniversary Article: Reversible and Adaptive Functional Supramolecular Materials: “Noncovalent Interaction” Matters. *Adv. Mater.* **2013**, *25*, 5530–5548.

9 Yang, L.; Tan, X.; Wang, Z.; Zhang, X. Supramolecular Polymers: Historical Development, Preparation, Characterization, and Functions. *Chem. Rev.* **2015**, *115*, 7196–7239.

10 Amabilino, D. B.; Smith, D. K.; Steed, J. W. Supramolecular Materials. *Chem. Soc. Rev.* **2017**, *46*, 2404–2420.

11 Kuo, S.-W. Hydrogen Bonding in Polymeric Materials. In: *Hydrogen Bonding in Polymeric Materials*; Kuo, S.-W., Ed.; Wiley-VCH: Weinheim, Germany, **2018**; pp 1–8.

12 Zhang, X.; Wang, L.-Y.; Xu, J.; Chen, D.-Y.; Shi, L.-Q.; Zhou, Y.-F.; Shen, Z.-H.

Polymeric Supramolecular Systems: Design, Assembly and Functions. *Acta Polym. Sin.* **2019**, *50*, 973–987.

13 Qin, B.; Yin, Z.; Tang, X.; Zhang, S.; Wu, Y.; Xu, J.-F.; Zhang, X. Supramolecular Polymer Chemistry: From Structural Control to Functional Assembly. *Prog. Polym. Sci.* **2020**, *100*, 101167.

14 Sijbesma, R. P.; Beijer, F. H.; Brunsveld, L.; Folmer, B. J. B.; Hirschberg, J. H. K. K.; Lange, R. F. M.; Lowe, J. K. L.; Meijer, E. W. Reversible Polymers Formed from Self-Complementary Monomers Using Quadruple Hydrogen Bonding. *Science* **1997**, *278*, 1601–1604.

15 Beijer, F. H.; Sijbesma, R. P.; Kooijman, H.; Spek, A. L.; Meijer, E. W. Strong Dimerization of Ureidopyrimidones via Quadruple Hydrogen Bonding. *J. Am. Chem. Soc.* **1998**, *120*, 6761–6769.

16 Folmer, B. J. B.; Sijbesma, R. P.; Kooijman, H.; Spek, A. L.; Meijer, E. W. Cooperative Dynamics in Duplexes of Stacked Hydrogen-Bonded Moieties. *J. Am. Chem. Soc.* **1999**, *121*, 9001–9007.

17 Söntjens, S. H. M.; Sijbesma, R. P.; van Genderen, M. H. P.; Meijer, E. W. Stability and Lifetime of Quadruply Hydrogen Bonded 2-Ureido-4[1H]-pyrimidinone Dimers. *J. Am. Chem. Soc.* **2000**, *122*, 7487–7493.

18 Ligthart, G. B. W. L.; Ohkawa, H.; Sijbesma, R. P.; Meijer, E. W. Complementary Quadruple Hydrogen Bonding in Supramolecular Copolymers. *J. Am. Chem. Soc.* **2005**, *127*, 810–811.

19 Dankers, P. Y. W.; Van Leeuwen, E. N. M.; Van Gemert, G. M. L.; Spiering, A. J. H.; Harmsen, M. C.; Brouwer, L. A.; Janssen, H. M.; Bosman, A. W.; Van Luyn, M. J. A.; Meijer, E. W. Chemical and Biological Properties of Supramolecular Polymer Systems Based on Oligocaprolactones. *Biomaterials* **2006**, *27*, 5490–5501.

20 Faghihnejad, A.; Feldman, K. E.; Yu, J.; Tirrell, M. V.; Israelachvili, J. N.; Hawker, C. J.; Kramer, E. J.; Zeng, H. Adhesion and Surface Interactions of a Self-Healing Polymer with Multiple Hydrogen-Bonding Groups. *Adv. Funct. Mater.* **2014**, *24*, 2322–2333.

21 Heinzmann, C.; Lamparth, I.; Rist, K.; Moszner, N.; Fiore, G. L.; Weder, C. Supramolecular Polymer Networks Made by Solvent-Free Copolymerization of a Liquid 2-Ureido-4[1H]-Pyrimidinone Methacrylamide. *Macromolecules* **2015**, *48*, 8128–8136.

22 Murray, T. J.; Zimmerman, S. C. New Triply Hydrogen Bonded Complexes with Highly Variable Stabilities. *J. Am. Chem. Soc.* **1992**, *114*, 4010–4011.

23 Fenlon, E. E.; Murray, T. J.; Baloga, M. H.; Zimmerman, S. C. Convenient Synthesis of 2-Amino-1,8-Naphthyridines, Building Blocks for Host-Guest and Self-Assembling Systems. *J. Org. Chem.* **1993**, *58*, 6625–6628.

24 Zimmerman, S. C.; Murray, T. J., New Supramolecular Architectures Using Hydrogen Bonding. *Philos. Trans. R. Soc. A* **1993**, *345*, 49–56.

25 Zimmerman, S. C.; Murray, T. J. Hydrogen Bonded Complexes with the AA·DD, AA·DDD, and AAA·DD Motifs: The Role of Three Centered (Bifurcated) Hydrogen Bonding. *Tetrahedron. Lett.* **1994**, *35*, 4077–4080.

26 Murray, T. J.; Zimmerman, S. C.; Kolotuchin, S. V. Synthesis of Heterocyclic Compounds Containing Three Contiguous Hydrogen Bonding Sites in All Possible Arrangements. *Tetrahedron* **1995**, *51*, 635–648.

27 Murray, T. J.; Zimmerman, S. C. 7-Amido-1,8-Naphthyridines as Hydrogen Bonding Units for the Complexation of Guanine Derivatives: The Role of 2-Alkoxyl Groups in Decreasing Binding Affinity. *Tetrahedron Lett.* **1995,** *36*, 7627–7630.

28 Park, T.; Zimmerman, S. C. Interplay of Fidelity, Binding Strength, and Structure in Supramolecular Polymers. *J. Am. Chem. Soc.* **2006**, *128*, 14236–14237.

29 Yang, S. K.; Zimmerman, S. C. Hydrogen Bonding Modules for Use in Supramolecular Polymers. *Israel J. Chem.* **2013**, *53*, 511–520.

30 Djurdjevic, S.; Leigh, D. A.; McNab, H.; Parsons, S.; Teobaldi, G.; Zerbetto, F. Extremely Strong and Readily Accessible AAA–DDD Triple Hydrogen Bond Complexes. *J. Am. Chem. Soc.* **2007**, *129*, 476–477.

31 Blight, B. A.; Camara-Campos, A.; Djurdjevic, S.; Kaller, M.; Leigh, D. A.; McMillan, F. M.; McNab, H.; Slawin, A. M. AAA–DDD Triple Hydrogen Bond Complexes. *J. Am. Chem. Soc.* **2009**, *131*, 14116–14122.

32 Blight, B. A.; Hunter, C. A.; Leigh, D. A.; McNab, H.; Thomson, P. I. An AAAA–DDDD Quadruple Hydrogen-Bond Array. *Nat. Chem.* **2011**, *3*, 244–248.

33 Leigh, D. A.; Robertson, C. C.; Slawin, A. M. Z.; Thomson, P. I. AAAA-DDDD Quadruple Hydrogen-Bond Arrays Featuring NH···N and CH···N Hydrogen Bonds. *J. Am. Chem. Soc.* **2013**, *135*, 9939–9943.

34 Sijbesma, R. P.; Meijer, E. Quadruple Hydrogen Bonded Systems. *Chem. Commun.* **2003**, 5–16.

35 Wilson, A. J. Non-Covalent Polymer Assembly Using Arrays of Hydrogen-Bonds. *Soft Matter* **2007**, *3*, 409–425.

36 Coubrough, H. M.; Van der Lubbe, S. C. C.; Hetherington, K.; Minard, A.; Pask, C.; Howard, M. J.; Fonseca Guerra, C.; Wilson, A. J. Supramolecular Self-Sorting Networks Using Hydrogen-Bonding Motifs. *Chem. Eur. J.* **2019**, *25*, 785–795.

37 Braibanti, A.; Dallavalle, F.; Mori, G.; Pasquali, M. Chelate Effect and Cooperativity Effect in Metal-Ligand and Macromolecule-Ligand Equilibria. I. Chemical Potential Changes and Cooperativity-Chelation Parameters. *Inorg. Chim. Acta* **1984**, *91*, 195–201.

38 Ercolani, G.; Schiaffino, L. Allosteric, Chelate, and Interannular Cooperativity: A Mise au Point. *Angew. Chem. Int. Ed.* **2011**, *50*, 1762–1768.

39 Misuraca, M. C.; Grecu, T.; Freixa, Z.; Garavini, V.; Hunter, C. A.; Van Leeuwen, P. W. N. M.; Segarra-Maset, M. D.; Turega, S. M. Relationship Between Conformational Flexibility and Chelate Cooperativity. *J. Org. Chem.* **2011**, *76*, 2723–2732.

40 Hunter, C. A.; Misuraca, M. C.; Turega, S. M. Influence of H-bond Strength on Chelate Cooperativity. *J. Am. Chem. Soc.* **2011**, *133*, 20416–20425.

41 Hogben, H. J.; Sprafke, J. K.; Hoffmann, M.; Pawlicki, M.; Anderson, H. L. Stepwise Effective Molarities in Porphyrin Oligomer Complexes: Preorganization Results in Exceptionally Strong Chelate Cooperativity. *J. Am. Chem. Soc.* **2011**, *133*, 20962–20969.

42 Jorgensen, W. L.; Pranata, J. Importance of Secondary Interactions in Triply Hydrogen Bonded Complexes: Guanine-Cytosine vs Uracil-2,6-Diaminopyridine. *J. Am. Chem. Soc.* **1990**, *112*, 2008–2010.

43 Hunter, C. A.; Anderson, H. L. What is Cooperativity? *Angew. Chem. Int. Ed.* **2009**, *48*, 7488–7499.

44 Kassianidis, E.; Pearson, R. J.; Philp, D. Specific Autocatalysis in Diastereoisomeric Replicators. *Org. Lett.* **2005**, *7*, 3833–3836.

45 Kassiandis, E.; Philp, D. The design and implementation of a highly selective self-replicating system *Angew. Chem. Int. Ed.* **2006***, 45*, 6344–6348.

46 Kassiandis, E.; Pearson, R. J.; Philp, D. Probing structural effects on replication efficiency through comparative analyses of families of potential self-replicators *Chem Eur. J.* **2006**, *12*, 8788–8812.

47 Pearson, R. J.; Kassiandis, E.; Slawin, A. M. Z.; Philp, D. Comparative analyses of a family of potential self-replicators: the subtle interplay between molecular structure and the efficacy of self-replication *Chem Eur. J.* **2006***, 12,* 6829–6840.

48 Vidonne, A.; Philp, D. Making Molecules Make Themselves – The Chemistry of Artificial Replicators. *Eur. J. Org. Chem.* **2009**, *2009*, 593–610.

49 Kosikova, T.; Philp, D. Exploring the Emergence of Complexity Using Synthetic Replicators. *Chem. Soc. Rev.* **2017**, *46*, 7274–7305.

50 Del Amo, V.; Philp, D. Integrating Replication-Based Selection Strategies in Dynamic Covalent Systems. *Chem. Eur. J.* **2010**, *16*, 13304–13318.

51 Allen, V. C.; Robertson, C. C.; Turega, S. M.; Philp D. *A Simple network of synthetic replicators can perform the logical OR operation Org. Lett.* **2010**, *12*, 1920–1923.

52 Kosikova, T.; Philp, D. A critical crosscatalytic relationship determines the outcome of competition in a replicator network *J. Am. Chem. Soc.* **2017,** *139*, 12579–12590.

53 Sadownik, J. W.; Kosikova, T.; Philp, D. Generating system-level responses from a network of simple synthetic replicators *J. Am. Chem. Soc.* **2017,** *139*, 17565–17573.

54 Robertson, C. C.; Mackenzie, H. W.; Kosikova, T.; Philp, D. An Environmentally Responsive Reciprocal Replicating Network. *J. Am. Chem. Soc.* **2018**, *140*, 6832–6841.

55 Huck, J.; Kosikova, T.; Philp, D. Compositional Persistence in a Multicyclic Network of Synthetic Replicators *J. Am. Chem. Soc.* **2019,** *141*, 13905–13913.

56 Jencks, W. P. On the Attribution and Additivity of Binding Energies. *Proc. Natl. Acad. Sci. U. S. A.* **1981**, *78*, 4046–4050.

57 Liu, Y.; Wang, Z.; Zhang, X. Characterization of Supramolecular Polymers. *Chem. Soc. Rev.* **2012**, *41*, 5922-5932.

58 Scherman, O. A.; Ligthart, G. B. W. L.; Sijbesma, R. P.; Meijer, E. W. A Selectivity-Driven Supramolecular Polymerization of an AB Monomer. *Angew. Chem. Int. Ed.* **2006**, *45*, 2072–2076.

59 Huang, F.; Nagvekar, D. S.; Zhou, X.; Gibson, H. W. Formation of a Linear Supramolecular Polymer by Self-Assembly of Two Homoditopic Monomers Based on the Bis(*m*-Phenylene)-32-Crown-10/Paraquat Recognition Motif. *Macromolecules* **2007,** *40*, 3561–3567.

60 Niu, Z.; Huang, F.; Gibson, H. W., Supramolecular AA–BB-Type Linear Polymers with Relatively High Molecular Weights *via* the Self-Assembly of Bis(*m*-Phenylene)-32-Crown-10 Cryptands and a Bisparaquat Derivative. *J Am Chem Soc* **2011,** *133*, 2836-2839.

61 Wang, P.; Ma, J.; Xia, D. A H_2S and I^- Dual-Responsive Supramolecular Polymer Constructed *via* Pillar[5]arene-Based Host–Guest interactions and Metal Coordination. *Org. Chem. Front.* **2018**, *5*, 1297–1302.

62 Zhang, R.; Yan, X.; Guo, H.; Hu, L.; Yan, C.; Wang, Y.; Yao, Y. Supramolecular Polymer Networks Based on Pillar[5]arene: Synthesis, Characterization and Application in the Fenton Reaction. *Chem. Commun.* **2020**, *56*, 948–951.

63 Maugeri, L.; Lebl, T.; Cordes, D. B.; Slawin, A. M. Z.; Philp, D. *Cooperative Binding in a Phosphine Oxide-Based Halogen Bonded Dimer Drives Supramolecular Oligomerization J. Org. Chem.* **2017,** *82*, 1986–1995.

64 Griffith, J. S. Nature of the Scrapie Agent: Self-Replication and Scrapie. *Nature* **1967**, *215*, 1043–1044.

65 Rubinov, B.; Wagner, N.; Rapaport, H.; Ashkenasy, G. Self-Replicating Amphiphilic β-Sheet Peptides. *Angew. Chem. Int. Ed.* **2009**, *48*, 6683–6686.

66 Pal, A.; Malakoutikhah, M.; Leonetti, G.; Tezcan, M.; Colomb-Delsuc, M.; Nguyen, V. D.; van der Gucht, J.; Otto, S. Controlling the Structure and Length of Self-

Synthesizing Supramolecular Polymers through Nucleated Growth and Disassembly. *Angew. Chem. Int. Ed.* **2015**, *54*, 7852–7856.

67 Ashkenasy, G.; Hermans, T. M.; Otto, S.; Taylor, A. F. Systems Chemistry. *Chem. Soc. Rev.* **2017**,*46*, 2543–2554.

68 Frederix, P. W. J. M.; Idé, J.; Altay, Y.; Schaeffer, G.; Surin, M.; Beljonne, D.; Bondarenko, A. S.; Jansen, T. L. C.; Otto, S.; Marrink, S. J. Structural and Spectroscopic Properties of Assemblies of Self-Replicating Peptide Macrocycles. *ACS Nano* **2017**, *11*, 7858–7868.

69 Bartolec, B.; Altay, M.; Otto, S. Template-Promoted Self-Replication in Dynamic Combinatorial Libraries Made from a Simple Building Block. *Chem. Comm.* **2018**, *54*, 13096–13098.

70 Altay, Y.; Altay, M.; Otto, S. Existing Self-Replicators Can Direct the Emergence of New Ones. *Chem. Eur. J.* **2018**, *24*, 11911–11915.

71 Maity, S.; Ottelé, J.; Santiago, G. M.; Frederix, P. W. J. M.; Kroon, P.; Markovitch, O.; Stuart, M. C. A.; Marrink, S. J.; Otto, S.; Roos, W. H. Caught in the Act: Mechanistic Insight into Supramolecular Polymerization-Driven Self-Replication from Real-Time Visualization. *J. Am. Chem. Soc.* **2020**, *142*, 13709–13717.

72 Mishra, A.; Korlepara, D. B.; Kumar, M.; Jain, A.; Jonnalagadda, N.; Bejagam, K. K.; Balasubramanian, S.; George, S. J. Biomimetic Temporal Self-Assembly via Fuel-Driven Controlled Supramolecular Polymerization. *Nat. Commun.* **2018**, *9*, 1295.

73 Jain, A.; Dhiman, S.; Dhayani, A.; Vemula, P. K.; George, S. J. Chemical Fuel-Driven Living and Transient Supramolecular Polymerization. *Nat. Commun.* **2019**, *10*, 450.

74 Jalani, K.; Das, A. D.; Sasmal, R.; Agasti, S. S.; George, S. J. Transient dormant monomer states for supramolecular polymers with low dispersity. *Nat. Commun.* **2020**, *11*, 3967.

Table of Contents Graphic